Lattice-form-dependent orbital shape and charge disproportionation in charge- and orbital-ordered manganites

D. Okuyama,[1,2] Y. Tokunaga,[2] R. Kumai,[3] Y. Taguchi,[1] T. Arima,[4] and Y. Tokura[1,2,3,5]
[1]*Cross-Correlated Materials Research Group (CMRG), ASI, RIKEN, Wako 351-0198, Japan*
[2]*Multiferroics Project, ERATO, Japan Science and Technology Agency (JST), c/o RIKEN, Wako 351-0198, Japan*
[3]*National Institute of Advanced Industrial Science and Technology (AIST), Tsukuba 305-8562, Japan*
[4]*Institute of Multidisciplinary Research for Advanced Materials, Tohoku University, Sendai 980-8577, Japan*
[5]*Department of Applied Physics, University of Tokyo, Tokyo 113-8656, Japan*
(Received 26 April 2009; revised manuscript received 17 July 2009; published 6 August 2009)

The orbital shapes and charge disproportionations at nominal Mn^{3+} and Mn^{4+} sites for the charge- and orbital-ordered phases have been studied on half-doped manganites $Pr(Sr_{0.1}Ca_{0.9})_2Mn_2O_7$ and $Eu_{0.5}Ca_{1.5}MnO_4$ with double-layer and single-layer Mn-O networks, respectively, by means of x-ray structural analyses, in comparison with $Pr_{0.5}Ca_{0.5}MnO_3$ with the pseudocubic network. In a single-layer $Eu_{0.5}Ca_{1.5}MnO_4$ system, the $(y^2-z^2)/(z^2-x^2)$-type orbital shape is observed, while the $(3y^2-r^2)/(3x^2-r^2)$-type orbital shape in a pseudocubic $Pr_{0.5}Ca_{0.5}MnO_3$ system. In a double-layer $Pr(Sr_{0.1}Ca_{0.9})_2Mn_2O_7$ system, the orbital shape is found to undergo a large change upon thermally induced rotation of orbital stripe. Furthermore, clear charge disproportionation is observed for the pseudocubic and double-layer systems, while it is not observed in the single-layer system. These results indicate that the orbital shape and charge disproportionation are sensitive to the dimension of Mn-O network.

DOI: 10.1103/PhysRevB.80.064402 PACS number(s): 75.30.−m, 75.47.Lx, 61.05.cp

I. INTRODUCTION

Charge and orbital order (CO-OO) in mixed-valence manganites with perovskite-related structures has been attracting great interest since the CO-OO makes a strong impact on crystallography, magnetism, and electrical conduction.[1] For example, magnetic-field-induced melting of long-range and/or short-range CO-OO results in colossal magnetoresistance.[2] Huge changes in electrical conduction due to the melting of CO-OO have been reported with the application of other external stimuli, such as an electric field, x-ray, light, and pressure.[3–6] Many diffraction and theoretical studies have reported the checkerboard-type charge order of Mn^{3+} and Mn^{4+} ions with charge disproportionation and stripe-type orbital order explaining a complex antiferromagnetic spin order at low temperatures in half-doped manganites.[7–16] On the other hand, another model with less distinct charge disproportionation has also been proposed.[17–25] For example, taking into account the on-site Coulomb interaction, Brink *et al.*[17] have suggested that maximum value of charge disproportionation is as little as 20%. First-principle calculation by Mahadevan *et al.*[18] have also shown that the charge disproportionation is almost negligible for $La_{0.5}Sr_{1.5}MnO_4$ compound. Herrero-Martin *et al.*[21] have inferred from the resonant x-ray scattering data that the charge disproportionation of $Nd_{0.5}Sr_{0.5}MnO_3$ is about 20%. These different models have raised an important question about the nature of CO state.

Another issue to be clarified is the orbital shape at Mn^{3+} ion in the CO-OO phase. Radaelli *et al.*[26] suggested by powder neutron and synchrotron x-ray diffraction studies that the $(3y^2-r^2)/(3x^2-r^2)$-type orbital order takes place in $La_{0.5}Ca_{0.5}MnO_3$. $La_{0.5}Sr_{1.5}MnO_4$ was also studied as another CO-OO system by resonant x-ray scattering and x-ray linear dichroism methods;[10,27] the latter[27] strongly suggested the $(y^2-z^2)/(z^2-x^2)$-type orbital shape at Mn^{3+} ion. It is an unsolved problem why the orbital shape of $La_{0.5}Ca_{0.5}MnO_3$ and $La_{0.5}Sr_{1.5}MnO_4$ appear different. One obvious difference between these two materials is the dimensionality of MnO_6 network. The variation in the dimensionality has already been reported[28–30] to affect the CO-OO state significantly in terms of correlation length but its effect on the orbital shape should be investigated systematically. To clarify these issues, we have made systematic investigations on the charge disproportionation and orbital shape in the CO-OO phases of half-doped manganites with various Mn-O networks (single-, double-, and infinite-layered MnO_2 sheets) by means of x-ray structure analysis. The results indicate that the charge disproportionation is in reality much smaller than unity and that the orbital shape critically depends on the lattice form, in particular, on the dimensionality of Mn-O network. As far as we know, there has been no experimental investigation on the charge disproportionation for the layered manganites thus far.

The investigated materials in this study are $Pr_{0.5}Ca_{0.5}MnO_3$, $Pr(Sr_{0.1}Ca_{0.9})_2Mn_2O_7$, and $Eu_{0.5}Ca_{1.5}MnO_4$ with pseudocubic, double-layer, and single-layer Mn-O networks, respectively. We chose these materials with good size matching of the ionic radii at the *A* sites to reduce the effect of quenched disorder (randomness) as much as possible.[31–33] Another important point in selecting the target materials is that the well-defined orthorhombic distortion of all these materials enables us to obtain the single-domain orbital-ordered state as locked by the orthorhombicity. The concomitant CO-OO is observed at T_{CO} which is higher than the CE-type antiferromagnetic ordering in every case.[33,34] In $Pr_{0.5}Ca_{0.5}MnO_3$ and $Eu_{0.5}Ca_{1.5}MnO_4$, the CO-OO transitions take place at $T_{CO}\sim 230$ and 325 K, and the CE-type antiferromagnetic order with spins pointing along the *b* axis is established at $T_N\sim 170$ and 120 K, respectively.[34–37]

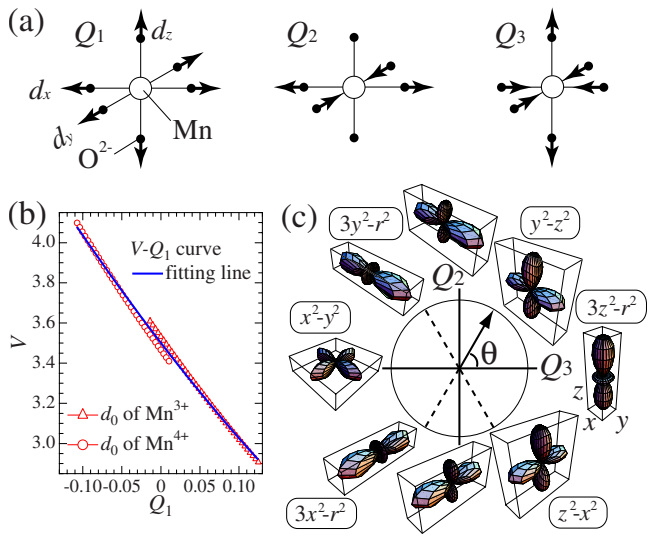

FIG. 1. (Color online) (a) Relevant distortion modes Q_1, Q_2, and Q_3 of a MnO_6 octahedron. Arrows indicate shifts in O^{2-} ions. (b) V-Q_1 curves calculated with using the bond valence sum formula. Triangles (circles) show the relation calculated for the d_0 value appropriate for an integer valence of Mn^{3+} (Mn^{4+}). A solid line indicates a quadratic fitting with the values of triangles and circles. (c) Preferred orbital shapes of an e_g electron with respect to the Q_2-Q_3 plane [Kanamori representation (Ref. 41)].

The ferromagnetic zigzag chain is parallel to the b axis in $Pr_{0.5}Ca_{0.5}MnO_3$ and to a axis in $Eu_{0.5}Ca_{1.5}MnO_4$, respectively. In contrast, successive CO-OO transitions are observed at $T_{CO1} \sim 370$ and $T_{CO2} \sim 315$ K in $Pr(Sr_{0.1}Ca_{0.9})_2Mn_2O_7$. The propagation direction of stripe-type orbital order spontaneously rotates from along the a axis to along the b axis at T_{CO2}; this appears as a generic feature of CO-OO double-layer manganites.[33] CE-type antiferromagnetic order with spins pointing along b axis grows below $T_N \sim 153$ K,[38] and the ferromagnetic zigzag chain is along a axis. In both of the $Eu_{0.5}Ca_{1.5}MnO_4$ and $Pr(Sr_{0.1}Ca_{0.9})_2Mn_2O_7$, CO-OO produces clear anisotropy of electronic states, typically manifested by the optical conductivity spectra, in which the oscillator strength at low energy region is more suppressed in orbital-stripe direction than in orbital zigzag chain direction[34,38]

II. EXPERIMENTS AND ANALYSES

We have performed structure analysis for single crystals of $Eu_{0.5}Ca_{1.5}MnO_4$ and $Pr(Sr_{0.1}Ca_{0.9})_2Mn_2O_7$ grown by the floating zone method. The crystals were crashed into small grains. X-ray diffraction experiments were performed for twin-free single crystals with a diameter of about 30 μm on the beamline BL-1A at Photon Factory in KEK, Japan. The photon energy of the incident x-rays was tuned at 18 keV ($\lambda = 0.688$ Å). X-ray beams were shaped into a square with the size of 300 μm $\times$ 300 μm by a collimator, which is enough larger than the size of samples. To detect x-rays, a large cylindrical imaging plate was utilized. Temperature was controlled by a nitrogen-gas-stream cryostat. The intensity data were operated to the F-tables by using the program

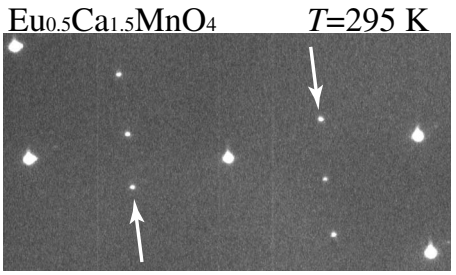

FIG. 2. Typical diffraction image of $Eu_{0.5}Ca_{1.5}MnO_4$ in the CO-OO phase (295 K). The arrows indicate the superlattice reflections, whose intensities are three orders of magnitude weaker than those of the bright fundamental spots.

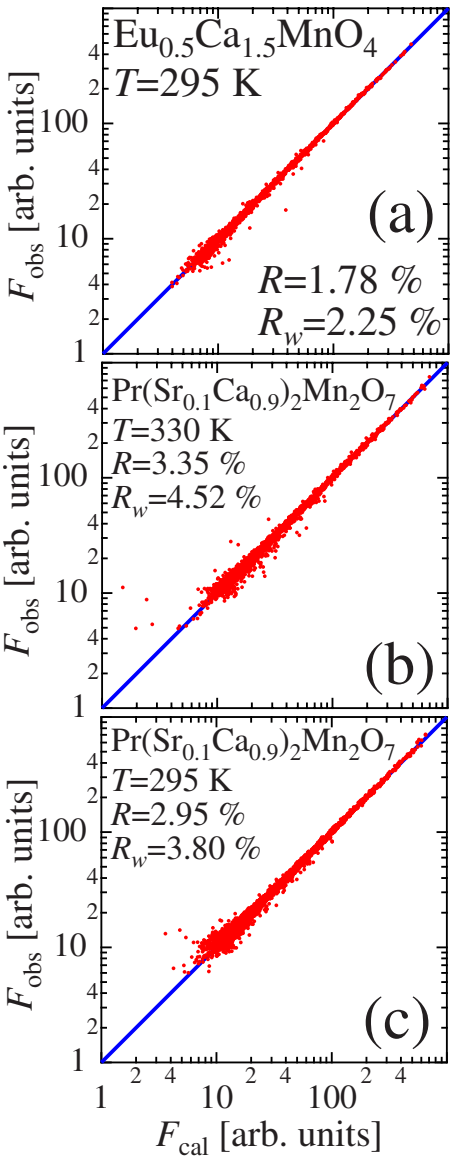

FIG. 3. (Color online) The comparison between observed (F_{obs}) and calculated (F_{cal}) structure factor of (a) $Eu_{0.5}Ca_{1.5}MnO_4$ at 295 K, (b) CO1 phase (330 K) of $Pr(Sr_{0.1}Ca_{0.9})_2Mn_2O_7$, and (c) CO2 phase (295 K) of $Pr(Sr_{0.1}Ca_{0.9})_2Mn_2O_7$, respectively.

of RAPID-AUTO, Rigaku Corp. and MSC. The SIR2004 program[39] was employed for the direct method. We used the program of CRYSTALSTRUCTURE of Rigaku Corp. and MSC. for analyzing the crystal structure from the F-table. Absorption effects were not corrected because the μr were enough small in each sample. For $Eu_{0.5}Ca_{1.5}MnO_4$ and $Pr(Sr_{0.1}Ca_{0.9})_2Mn_2O_7$, μr are $0.40(\mu=134.511\ cm^{-1})$ and $0.44(\mu=146.027\ cm^{-1})$, respectively. To check this assumption, we tried to correct the absorption effects. No difference was observed for the structural data obtained with and without the absorption correction.

For the analysis, we used thus determined crystal structure data for $Eu_{0.5}Ca_{1.5}MnO_4$ and $Pr(Sr_{0.1}Ca_{0.9})_2Mn_2O_7$, and the published data for $Pr_{0.5}Ca_{0.5}MnO_3$ by Goff *et al.*[22] We adopt the localized-orbital picture assuming *a priori* the strong electron-lattice interaction.[40] Then, the breathing and Jahn-Teller distortion modes, Q_1, Q_2, and Q_3, can be related with charge disproportionation and orbital shape[41] and can be defined as

$$\begin{pmatrix} Q_1 \\ Q_2 \\ Q_3 \end{pmatrix} = 1/\sqrt{6}\begin{pmatrix} \sqrt{2} & \sqrt{2} & \sqrt{2} \\ \sqrt{3} & -\sqrt{3} & 0 \\ -1 & -1 & 2 \end{pmatrix}\begin{pmatrix} d_x - \bar{d} \\ d_y - \bar{d} \\ d_z - \bar{d} \end{pmatrix}, \qquad (1)$$

where d_x, d_y, and d_z are bond lengths between Mn and O ions along the x, y, and z axes, respectively, which are shown as schematic views of distorted MnO_6 octahedra in Fig. 1(a). $\bar{d}=1.956(2)$ Å is the average bond length for $Mn^{3.5+}$ (Ref. 42). The approximate valences of Mn sites can be calculated from the bond valence sum[43] given by $V=\Sigma_i \exp[(d_0-d_i)/B]$. Here, V is the calculated valence, d_i is the ith Mn-O bond length, $d_0=1.760$ Å for Mn^{3+} and 1.753 Å for Mn^{4+}, and $B\sim 0.37$ Å.[43] Basically, the bond valence sum is appropriate for ions with formal valence of integer such as Mn^{3+} and Mn^{4+} ions. To estimate the bond valence sum of intermediate valence states, we use a quadratic fit with the bond valence sum curves for Mn^{3+} and Mn^{4+} as shown in Fig. 1(b).[44] On the other hand, it has been well known as Kanamori representation[41] that the orbital shape is related with the Jahn-Teller Q_2 and Q_3 modes, as shown in Fig. 1(c). In the Q_2-Q_3 plane, the orbital state is thus described as $|d_\theta\rangle=\cos(\frac{\theta}{2})|d_{3z^2-r^2}\rangle+\sin(\frac{\theta}{2})|d_{x^2-y^2}\rangle$. Similar analysis based on the bond valence sum and the Kanamori representation has been applied to manganites in some literatures.[22,45–47]

III. RESULTS

In Fig. 2, we show a typical diffraction pattern of $Eu_{0.5}Ca_{1.5}MnO_4$ in the CO-OO phase. Besides the fundamental Bragg spots, superlattice spots (indicated by arrows) due to cooperative Jahn-Teller distortion are clearly observed. The intensities of the superlattice reflections are three orders of magnitude weaker than those of the fundamental Bragg spots. There was no diffuse scattering intensity discerned around the superlattice spots indicating the minimal effect of quenched disorder.[48] In Figs. 3(a)–3(c), observed structure factor (F_{obs}) is plotted against the calculated one (F_{cal}) for $Eu_{0.5}Ca_{1.5}MnO_4$ at 295 K and for $Pr(Sr_{0.1}Ca_{0.9})_2Mn_2O_7$ at 330 and 295 K, respectively. The obtained reliability factors are $R=1.78\%$ and $R_w=2.25\%$ at CO-OO phase of $Eu_{0.5}Ca_{1.5}MnO_4$, $R=3.35\%$ and $R_w=4.52\%$ at CO1 phase ($T_{CO2}\leqq T\leqq T_{CO1}$), and $R=2.95\%$ and $R_w=3.80\%$ at CO2 phase ($T\leqq T_{CO2}$) of $Pr(Sr_{0.1}Ca_{0.9})_2Mn_2O_7$, respectively. De-

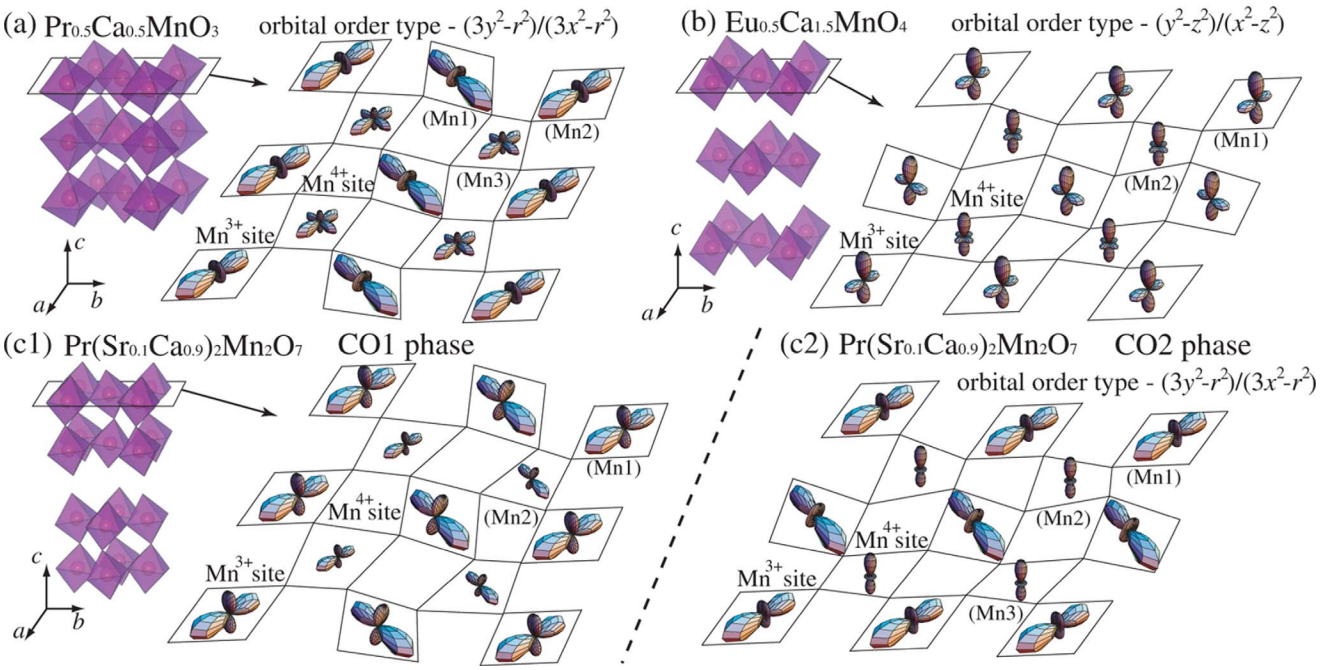

FIG. 4. (Color online) The CO-OO states schematically displayed for (a) $Pr_{0.5}Ca_{0.5}MnO_3$, (b) $Eu_{0.5}Ca_{1.5}MnO_4$, and (c1) CO1 phase (330 K) and (c2) CO2 phase (295 K) of $Pr(Sr_{0.1}Ca_{0.9})_2Mn_2O_7$. The crystal structural data reported by Goff *et al.* (Ref. 22) were used in the analysis of $Pr_{0.5}Ca_{0.5}MnO_3$.

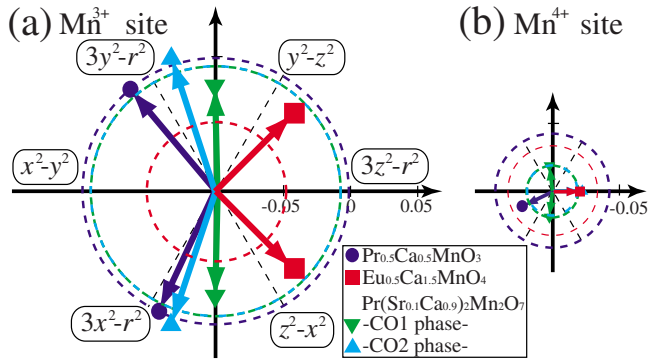

FIG. 5. (Color online) Orbital shapes and charge states of (a) Mn^{3+} and (b) Mn^{4+} sites. The radius of the circle is related to the Mn valence. The directions of arrows indicate the corresponding orbital shape.

tailed crystal structural data are listed in the Appendix and elsewhere.[49]

Figure 4(a) shows a schematic view of the CO-OO state of $Pr_{0.5}Ca_{0.5}MnO_3$, which is based on the crystal structural data by Goff *et al.*,[22] in which the space group and the lattice parameters at 10 K are reported to be $P2_1/m$ (No.11), $a=5.43499(3)$ Å, $b=10.8700(2)$ Å, and $c=7.488923(6)$ Å, respectively. Orbital stripes appear along the a axis, which is parallel to the diagonal-glide plane of the orbital-disordered phase. The orbital shapes at Mn^{3+} and Mn^{4+} sites of $Pr_{0.5}Ca_{0.5}MnO_3$ obtained by the present analysis are indicated in Figs. 5(a) and 5(b), respectively, in which the radius of the circle is related to Q_1 [$Q_1=-0.1$ (0.1) corresponds to $V\sim+4$ (+3)] and the direction of each arrow indicates the orbital state $|d_\theta\rangle$ calculated from Q_2 and Q_3. There are two crystallographically inequivalent Mn^{3+} sites termed Mn1 and Mn2, and one Mn^{4+} site (Mn3) in the CO-OO phase. The obtained values of d_x, d_y, d_z, Q_1, Q_2, Q_3, V, and θ are listed in Table I.[50] From these values, charge disproportionation between nominal Mn^{3+} and Mn^{4+} sites is estimated to be roughly 22%, which is very close to the value reported for $Nd_{0.5}Sr_{0.5}MnO_3$ using resonant x-ray scattering technique.[21] Furthermore, for the Mn1 and Mn2 sites, the $(3y^2-r^2)/(3x^2-r^2)$-type orbital shapes are obtained. For the Mn3 site, by contrast, the Q_2 and Q_3 values are small as compared to Q_1 value indicating the least Jahn-Teller distortion or unlifted orbital degeneracy with almost isotropic electron density, namely, $\rho(\boldsymbol{r})\propto\lambda|\Psi_{3z^2-r^2}|^2+|\Psi_{x^2-y^2}|^2$ with λ slightly smaller than 1.

The CO-OO state of $Eu_{0.5}Ca_{1.5}MnO_4$ with single-layer Mn-O network is schematically illustrated in Fig. 4(b). The crystal structural analysis showed that the space group is *Pmnb* (No.62) of orthorhombic crystal system and the lattice parameters are $a=10.6819(7)$ Å, $b=5.4071(3)$ Å, and $c=11.7018(11)$ Å at 295 K, respectively. Orbital stripes line up along the b axis, which is perpendicular to the diagonal-glide plane, giving rise to the observed optical anisotropy.[34] The obtained parameters are listed in Table II. About 8% charge disproportionation between Mn^{3+} and Mn^{4+} sites is observed, which should be interpreted as indicating that the actual charge disproportionation is almost negligible, taking into account the semiquantitative nature of the bond valence sum analysis. The negligible charge disproportionation is in excellent accord with the theoretical prediction[18] for the single-layer compound $La_{0.5}Sr_{1.5}MnO_4$. For Mn1 site, the $(y^2-z^2)/(x^2-z^2)$-type orbital shape is observed, as shown in Fig. 5. This orbital shape is also consistent with the result of x-ray linear dichroism experiment.[27] In contrast, for Mn2 site, Q_2 and Q_3 values are small with respect to Q_1 value indicating almost isotropic electron density $\rho(\boldsymbol{r})\propto\lambda|\Psi_{3z^2-r^2}|^2+|\Psi_{x^2-y^2}|^2$ with λ slightly larger than 1. Therefore, Mn1 and Mn2 sites can be regarded as nominal Mn^{3+} and Mn^{4+} site in the light of orbital activity, albeit, minimal charge disproportionation.

The pseudocubic and single-layer compounds show clear contrast in orbital shape and charge disproportionation; 22% charge disproportionation and $(3y^2-r^2)/(3x^2-r^2)$-type orbital shape of Mn^{3+} site for pseudocubic, while negligibly small charge disproportionation and $(y^2-z^2)/(x^2-z^2)$-type orbital shape for single-layer. From the crystallographic point of view, the double-layer system has an intermediate structure between pseudocubic and single-layer. We show in Fig. 4(c) schematic pictures of the CO-OO states of $Pr(Sr_{0.1}Ca_{0.9})_2Mn_2O_7$ with double-layer Mn-O network based on the structural parameters listed in Table III. The space groups are *Pbnm* (No.62) with $a=5.4087(2)$ Å, $b=10.9171(5)$ Å, and $c=19.2312(12)$ Å at 330 K (CO1) and *Am2m* (No.38) with $a=10.8026(7)$ Å, $b=5.4719(4)$ Å, and $c=19.2090(10)$ Å at 295 K (CO2), respectively. In the CO1 phase, the orbital stripes along the a axis are clearly seen, which is parallel to the diagonal-glide plane. We observe about 39% charge disproportionation in the CO1 phase. For Mn1 site, the orbital shape is of intermediate type between $(3y^2-r^2)/(3x^2-r^2)$ and $(y^2-z^2)/(z^2-x^2)$, and the similar orbital shape is obtained for Mn2 site (Fig. 5). $Pr(Sr_{0.1}Ca_{0.9})_2Mn_2O_7$ undergoes a transition with 90° rota-

TABLE I. Distortion of MnO_6 octahedra in $Pr_{0.5}Ca_{0.5}MnO_3$ at 10 K (Ref. 22). d_i and Q_j ($i=x, y, z$; $j=1,2,3$) are in Å. V and θ indicate the valence of Mn ion calculated from bond valence sum and an angle representing the orbital shape in the Q_2-Q_3 plane as exemplified in Fig. 1(c), respectively. The space group is $P2_1/m$ (No.11) and the lattice parameters are $a=5.43499(3)$ Å, $b=10.8700(2)$ Å, and $c=7.488923(6)$ Å, respectively.

	d_x	d_y	d_z	Q_1	Q_2	Q_3	V	θ
Mn1	2.039(6)	1.930(5)	1.9061(6)	0.004(4)	0.077(4)	−0.064(5)	3.48(2)	130(4)°
Mn2	1.911(8)	2.027(5)	1.9216(3)	−0.005(5)	−0.082(5)	−0.039(6)	3.53(3)	245(5)°
Mn3	1.933(5)	1.948(6)	1.914(3)	−0.042(6)	−0.011(6)	−0.021(6)	3.72(4)	21(2)×10°

TABLE II. Distortion of MnO_6 octahedra in $Eu_{0.5}Ca_{1.5}MnO_4$ at 295 K. The space group is *Pmnb* (No.62) of orthorhombic crystal system and the lattice parameters are $a=10.6819(7)$ Å, $b=5.4071(3)$ Å, and $c=11.7018(11)$ Å, respectively.

	d_x	d_y	d_z	Q_1	Q_2	Q_3	V	θ
Mn1	1.943(4)	1.863(3)	1.972(5)	−0.052(3)	0.057(3)	0.056(3)	3.77(2)	45(3)°
Mn2	1.910(5)	1.910(5)	1.934(4)	−0.066(3)	0.000(3)	0.019(3)	3.85(2)	0(1)×10°

tion of orbital stripes at $T_{CO2}\sim 315$ K.[38] In the CO2 phase, the orbital stripes run along the *b* axis, as clearly seen in Fig. 4(c2), in accord with the previous report.[38] There are one Mn^{3+} site and two crystallographically inequivalent Mn^{4+} sites termed, respectively, Mn1, Mn2, and Mn3 in the CO2 phase. The obtained charge disproportionation of about 39% is comparable with that of CO1 phase, whereas the $(3y^2-r^2)/(3x^2-r^2)$-type orbital shape as in $Pr_{0.5}Ca_{0.5}MnO_3$ is suggested for the Mn^{3+} sites as shown in Fig. 5. In both phases, the observed direction of orbital stripes is consistent with the optical anisotropy.[38]

IV. DISCUSSION

While the stripe-type orbital pattern commonly observed in the three materials gives rise to the same CE-type magnetic ordering, the orbital shape does depend on the structural difference and seems to be governed by the difference in the stacking sequence of (rare-earth/alkaline-earth)-oxygen (AO) planes and MnO_2 planes. Note that the AO plane contains apical oxygens of MnO_6 octahedra. In the charge- and orbital-disordered phase of $Pr_{0.5}Ca_{0.5}MnO_3$, MnO_6 octahedron is almost isotropic with slight compression along *c* axis due to the pseudocubic symmetry of the crystal structure.[37] Below the CO-OO transition, e_g electrons tend to maximize the kinetic-energy gain due to the local double exchange interaction with the neighboring Mn^{4+} t_{2g} spins on the *ab* plane and the $(3y^2-r^2)/(3x^2-r^2)$-type orbital shape is favored. In $Eu_{0.5}Ca_{1.5}MnO_4$, by contrast, the bond length between Mn and apical oxygen is longer than that within the plane even in the charge- and orbital-disordered phase at 360 K (see table in the Appendix). This is because a single MnO_2 plane is negatively charged and, hence, apical oxygen and rare-earth/alkaline-earth ions on the adjacent layers tend to be apart from and close to the MnO_2 plane, respectively. The body-centered nature of the K_2NiF_4-type structure allows this type of local lattice distortion in a cooperative manner. [It should be noted that this lattice distortion is not driven by the Jahn-Teller interaction, but due to the purely lattice structural effect, as evidenced by the presence of similar lattice distortion in La_2NiO_4 (Ref. 51) in which Ni^{2+} (with two e_g electrons) with $S=1$ is Jahn-Teller inactive.] Therefore, the electron orbital extended along the *c* axis is stabilized by such a distortion at high temperatures. As the temperature is lowered, however, e_g electrons tend to favor the orbital shape extended within the MnO_2 planes so as to gain the spin-exchange energy, similar to the case of $Pr_{0.5}Ca_{0.5}MnO_3$, thereby establishing $(y^2-z^2)/(z^2-x^2)$-type orbital order at T_{CO}. The structure of $Pr(Sr_{0.1}Ca_{0.9})_2Mn_2O_7$ compound can be viewed as intermediate between the single-layer and infinite-layer compounds. Therefore, it is likely that an intermediate orbital state between $Pr_{0.5}Ca_{0.5}MnO_3$ and $Eu_{0.5}Ca_{1.5}MnO_4$ is favored in the intermediate CO1 phase. In the CO2 phase, however, the $(3y^2-r^2)/(3x^2-r^2)$-type orbital shape is realized as in the pseudocubic case in which the magnetic interaction as favoring the CE-type order may play a role.

As the layer number is increased, charge disproportionation increases from the smallest value of 8% for the single-layer compound to 39% for the double-layer material and then rather decreases to 22% for the infinite-layer compound. In the single-layer system, the development of order parameter may be suppressed due to the enhanced fluctuation effect. In the double-layer system, fluctuation effect would be reduced and the larger charge disproportionation is observed. The reason why the observed charge disproportionation is smaller in the infinite-layer material than in double-layer

TABLE III. Distortion of MnO_6 octahedra at CO1 phase (330 K) and CO2 phase (295 K) of $Pr(Sr_{0.1}Ca_{0.9})_2Mn_2O_7$. The space group is *Pbnm* (No.62) and *Am2m* (No.38) of orthorhombic crystal system at 330 K and 295 K, respectively, and the lattice parameters are $a=5.4087(2)$ Å, $b=10.9171(5)$ Å, and $c=19.2312(12)$ Å at 330 K and $a=10.8026(7)$ Å, $b=5.4719(4)$ Å, and $c=19.2090(10)$ Å at 295 K, respectively.

330 K	d_x	d_y	d_z	Q_1	Q_2	Q_3	V	θ
Mn1	2.007(4)	1.899(3)	1.952(4)	−0.006(3)	0.076(3)	−0.001(3)	3.53(2)	91(3)°
Mn2	1.898(4)	1.925(5)	1.908(4)	−0.080(3)	0.019(3)	−0.003(3)	3.92(2)	10(1)×10°
295 K	d_x	d_y	d_z	Q_1	Q_2	Q_3	V	θ
Mn1	2.032(2)	1.898(2)	1.926(3)	−0.007(2)	0.095(2)	−0.032(2)	3.53(2)	109(1)°
Mn2	1.901(2)	1.901(2)	1.929(3)	−0.080(2)	0.000(2)	0.023(2)	3.92(2)	0(5)°
Mn3	1.905(2)	1.905(2)	1.924(3)	−0.077(2)	0.000(2)	0.016(2)	3.91(2)	0(8)°

compound is not clear at present, but the enhanced double exchange interaction in the infinite-layer material due to the increased dimensionality might be the origin.

V. SUMMARY

In summary, we have revealed that the charge disproportionation between nominal Mn^{3+} and Mn^{4+} is in reality much smaller than unity and, in particular, negligible in single-layer system. This result is in contrast with the belief at the early stage of the research of the CO-OO phenomena but in accord with the recent results.[16–25] This indicates that various interactions, such as electron-lattice, Coulomb repulsion, and magnetic interactions, should be taken into account to correctly understand the nature of charge-ordered state. The orbital shape is different among the three compounds despite the same symmetry of the CO-OO pattern in a single MnO_2 plane, structurally confirming the previous conclusions based on different experimental techniques.[26,27] The charge disproportionation and orbital shape in these materials are dominated by the dimension of Mn-O network and the local environment of the apical oxygen seems to be particularly important.

ACKNOWLEDGMENTS

The authors thank S. Ishiwata and Y. Tomioka for fruitful discussions. This study was performed with the approval of the Photon Factory Program Advisory Committee (No.2006S2-005).

APPENDIX: CRYSTAL-STRUCTURAL DATA

We present the crystal structural data of $Eu_{0.5}Ca_{1.5}MnO_4$ and $Pr(Sr_{0.1}Ca_{0.9})_2Mn_2O_7$. The crystal structural data at 360 (disordered phase) and 295 K (CO-OO phase) of $Eu_{0.5}Ca_{1.5}MnO_4$ are shown in Table IV and EPAPS,[49] respectively. From the crystal data, the distortion parameters of 360 K is calculated and summarized as Table V. For $Pr(Sr_{0.1}Ca_{0.9})_2Mn_2O_7$, the crystal structure data in disordered phase (at 405 K) is presented in Table VI. For two CO-OO phases, the data at 330 K in CO1 phase ($T_{CO2} \leqq T \leqq T_{CO1}$) and at 295 K in CO2 ($T \leqq T_{CO2}$) are listed in EPAPS.[49] In Table VII, the distortion parameters at 405 K is reported. In these crystal structural data, x, y, and z indicate the fractional coordinates. g is the site-occupation number. Anisotropic atomic-displacement parameters are represented as U_{11}, U_{22}, U_{33}, U_{12}, U_{13}, and U_{23}, while B_j and $\langle u_j^2 \rangle$ ($B_j = 8\pi^2 U_j = 8\pi^2 \langle u_j^2 \rangle$) are the isotropic atomic displacement parameter and the mean-square atomic displacement of the ion j, respectively. From the B_j, the Debye-Waller factor is expressed as $\exp(-B_j(\sin\theta_K/\lambda)^2)$, where θ_K and λ are the Bragg angle and wavelength, respectively.

TABLE IV. The structure parameters of $Eu_{0.5}Ca_{1.5}MnO_4$ in the disordered phase at 360 K. 3048 reflections were observed, and 966 of them are independent. The 29 variables were used for the refinement. The space group is *Bmab* (No.64) of orthorhombic crystal system. The latticce parameters are as follows: a =5.3638(19) Å, b=5.4088(9) Å, and c=11.738(2) Å. The reliability factors are R=2.40%, R_w=2.55%, and goodness of fit (GOF) GOF=1.062.

	Site	x	y	z	g	B (Å^2)
Eu1	8f	0	0.9933(4)	0.64219(16)	1/4	0.645(15)
Ca1	8f	0	0.9854(5)	0.6427(2)	3/4	0.75(2)
Mn	4a	0	0	0	1	0.412(5)
O1	8e	1/4	3/4	0.98777(8)	1	1.097(19)
O2	8f	0	0.9623(2)	0.16570(7)	1	1.51(2)
	U_{11} (Å^2)	U_{22} (Å^2)	U_{33} (Å^2)	U_{12} (Å^2)	U_{13} (Å^2)	U_{23} (Å^2)
Eu1	0.0111(8)	0.00898(17)	0.0044(2)	0.0000	0.0000	0.00132(14)
Ca1	0.0129(9)	0.0097(2)	0.0060(3)	0.0000	0.0000	−0.00106(19)
Mn	0.0056(2)	0.00414(4)	0.00593(6)	0.0000	0.0000	−0.00030(2)
O1	0.0111(10)	0.01142(19)	0.0192(2)	0.0028(3)	0.0000	0.0000
O2	0.0314(11)	0.0202(3)	0.00583(15)	0.0000	0.0000	−0.00107(19)

TABLE V. Distortion of MnO_6 octahedra in $Eu_{0.5}Ca_{1.5}MnO_4$ at 360 K (disordered phase). V and θ are the same as in Table I.

360 K	d_x	d_y	d_z	Q_1	Q_2	Q_3	V	θ
Mn1	1.9098(4)	1.9098(4)	1.9556(9)	−0.054(2)	0.000(2)	0.037(2)	3.78(2)	0(3)°

TABLE VI. The structure parameters of $Pr(Sr_{0.1}Ca_{0.9})_2Mn_2O_7$ in the disordered phase at 405 K. 6074 reflections were observed and 2088 of them are independent. The 48 variables were used for the refinement. The space group is *Amam* (No.63) of orthorhombic crystal system. The lattice parameters are as follows: $a=5.4080(5)$ Å, $b=5.4599(5)$ Å, and $c=19.266(3)$ Å. The reliability factors are $R=3.42\%$, $R_w=4.31\%$, and GOF=1.088.

	Site	x	y	z	g	B (Å^2)
Pr1	8g	3/4	0.2375(6)	0.1844(2)	0.21	0.86(2)
Pr2	4c	3/4	0.25011(18)	0	0.58	0.763(16)
Sr1	8g	3/4	0.2413(5)	0.1833(2)	0.08	0.73(2)
Sr2	4c	3/4	0.2523(8)	0	0.04	1.11(7)
Ca1	8g	3/4	0.2413(5)	0.1833(2)	0.71	0.73(2)
Ca2	4c	3/4	0.2523(8)	0	0.38	1.11(7)
Mn	8g	3/4	0.74812(2)	0.09956(2)	1	0.484(3)
O1	8e	0	1/2	0.10744(12)	1	1.42(2)
O2	8e	0	0	0.08776(11)	1	1.33(2)
O3	8g	3/4	0.7950(2)	0.19846(11)	1	1.37(2)
O4	4c	3/4	0.6950(4)	0	1	1.52(4)
	U_{11} (Å^2)	U_{22} (Å^2)	U_{33} (Å^2)	U_{12} (Å^2)	U_{13} (Å^2)	U_{23} (Å^2)
Pr1	0.0156(7)	0.0111(4)	0.0059(13)	0.0000	0.0000	0.0006(5)
Pr2	0.0126(3)	0.0106(2)	0.0059(6)	0.0000	0.0000	0.0000
Sr1	0.0087(10)	0.0103(3)	0.0087(3)	0.0000	0.0000	0.0005(4)
Sr2	0.0062(9)	0.0096(10)	0.026(3)	0.0000	0.0000	0.0000
Ca1	0.0087(10)	0.0103(3)	0.0087(3)	0.0000	0.0000	0.0005(4)
Ca2	0.0062(9)	0.0096(10)	0.026(3)	0.0000	0.0000	0.0000
Mn	0.00527(6)	0.00597(5)	0.00715(15)	0.0000	0.0000	−0.00005(4)
O1	0.0150(4)	0.0164(3)	0.0226(11)	0.0062(2)	0.0000	0.0000
O2	0.0158(4)	0.0165(3)	0.0182(11)	−0.0046(3)	0.0000	0.0000
O3	0.0263(6)	0.0176(4)	0.0080(10)	0.0000	0.0000	−0.0008(4)
O4	0.0325(10)	0.0164(5)	0.0090(14)	0.0000	0.0000	0.0000

TABLE VII. Distortion of MnO_6 octahedra at 405 K (disorder phase) of $Pr(Sr_{0.1}Ca_{0.9})_2Mn_2O_7$.

405 K	d_x	d_y	d_z	Q_1	Q_2	Q_3	V	θ
Mn1	1.9309(3)	1.9309(3)	1.931(2)	−0.043(2)	0.000(2)	0.000(2)	3.72(2)	0°

[1] Y. Tokura and N. Nagaosa, Science **288**, 462 (2000).
[2] Y. Tokura, Rep. Prog. Phys. **69**, 797 (2006).
[3] A. Asamitsu, Y. Tomioka, H. Kuwahara, and Y. Tokura, Nature (London) **388**, 50 (1997).
[4] V. Kiryukhin, D. Casa, J. P. Hill, B. Keimer, A. Vigliante, Y. Tomioka, and Y. Tokura, Nature (London) **386**, 813 (1997).
[5] M. Fiebig, K. Miyano, Y. Tomioka, and Y. Tokura, Science **280**, 1925 (1998).
[6] Y. Moritomo, H. Kuwahara, Y. Tomioka, and Y. Tokura, Phys. Rev. B **55**, 7549 (1997).
[7] E. O. Wollan and W. C. Koehler, Phys. Rev. **100**, 545 (1955).
[8] J. B. Goodenough, Phys. Rev. **100**, 564 (1955).
[9] C. H. Chen and S.-W. Cheong, Phys. Rev. Lett. **76**, 4042 (1996).
[10] Y. Murakami, H. Kawada, H. Kawata, M. Tanaka, T. Arima, Y. Moritomo, and Y. Tokura, Phys. Rev. Lett. **80**, 1932 (1998).
[11] I. V. Solovyev and K. Terakura, Phys. Rev. Lett. **83**, 2825 (1999).
[12] T. Mutou and H. Kontani, Phys. Rev. Lett. **83**, 3685 (1999).
[13] C. H. Chen, S. Mori, and S.-W. Cheong, Phys. Rev. Lett. **83**, 4792 (1999).
[14] D. Khomskii and J. van den Brink, Phys. Rev. Lett. **85**, 3329 (2000).
[15] E. Dagotto, T. Hotta, and A. Moreo, Phys. Rep. **344**, 1 (2001).
[16] Z. Popović and S. Satpathy, Phys. Rev. Lett. **88**, 197201 (2002).
[17] J. van den Brink, G. Khaliullin, and D. Khomskii, Phys. Rev. Lett. **83**, 5118 (1999).
[18] P. Mahadevan, K. Terakura, and D. D. Sarma, Phys. Rev. Lett. **87**, 066404 (2001).
[19] G. Subías, J. García, M. G. Proietti, and J. Blasco, Phys. Rev. B **56**, 8183 (1997).

[20] J. García, M. C. Sánchez, G. Subías, and J. Blasco, J. Phys.: Condens. Matter **13**, 3229 (2001).
[21] J. Herrero-Martín, J. García, G. Subías, J. Blasco, and M. C. Sánchez, Phys. Rev. B **70**, 024408 (2004).
[22] R. J. Goff and J. P. Attfield, Phys. Rev. B **70**, 140404(R) (2004).
[23] J. C. Loudon, S. Cox, A. J. Williams, J. P. Attfield, P. B. Littlewood, P. A. Midgley, and N. D. Mathur, Phys. Rev. Lett. **94**, 097202 (2005).
[24] G. C. Milward, M. J. Calderón, and P. B. Littlewood, Nature (London) **433**, 607 (2005).
[25] S. Cox, J. Singleton, R. D. Mcdonald, A. Migliori, and P. B. Littlewood, Nature Mater. **7**, 25 (2008).
[26] P. G. Radaelli, D. E. Cox, M. Marezio, and S.-W. Cheong, Phys. Rev. B **55**, 3015 (1997).
[27] D. J. Huang, W. B. Wu, G. Y. Guo, H.-J. Lin, T. Y. Hou, C. F. Chang, C. T. Chen, A. Fujimori, T. Kimura, H. B. Huang, A. Tanaka, and T. Jo, Phys. Rev. Lett. **92**, 087202 (2004).
[28] M. v. Zimmermann, J. P. Hill, D. Gibbs, M. Blume, D. Casa, B. Keimer, Y. Murakami, Y. Tomioka, and Y. Tokura, Phys. Rev. Lett. **83**, 4872 (1999).
[29] Y. Wakabayashi, Y. Murakami, Y. Moritomo, I. Koyama, H. Nakao, T. Kiyama, T. Kimura, Y. Tokura, and N. Wakabayashi, J. Phys. Soc. Jpn. **70**, 1194 (2001).
[30] O. Zachar and I. Zaliznyak, Phys. Rev. Lett. **91**, 036401 (2003).
[31] Y. Tomioka and Y. Tokura, Phys. Rev. B **70**, 014432 (2004).
[32] R. Mathieu, M. Uchida, Y. Kaneko, J. P. He, X. Z. Yu, R. Kumai, T. Arima, Y. Tomioka, A. Asamitsu, Y. Matsui, and Y. Tokura, Phys. Rev. B **74**, 020404(R) (2006).
[33] Y. Tokunaga, T. J. Sato, M. Uchida, R. Kumai, Y. Matsui, T. Arima, and Y. Tokura, Phys. Rev. B **77**, 064428 (2008).
[34] Y. Tokunaga, R. Kumai, N. Takeshita, Y. Kaneko, J. P. He, T. Arima, and Y. Tokura, Phys. Rev. B **78**, 155105 (2008).
[35] Z. Jirák, S. Krupička, Z. Šimša, M. Dlouhá, and S. Vratislav, J. Magn. Magn. Mater. **53**, 153 (1985).
[36] Y. Tomioka, A. Asamitsu, H. Kuwahara, Y. Moritomo, and Y. Tokura, Phys. Rev. B **53**, R1689 (1996).
[37] Z. Jirák, F. Damay, M. Hervieu, C. Martin, B. Raveau, G. André, and F. Bourée, Phys. Rev. B **61**, 1181 (2000).
[38] Y. Tokunaga, T. Lottermoser, Y. Lee, R. Kumai, M. Uchida, T. Arima, and Y. Tokura, Nature Mater. **5**, 937 (2006).
[39] M. C. Burla, R. Caliandro, M. Camalli, B. Carrozzini, G. L. Cascarano, L. De Caro, C. Giacovazzo, G. Polidori, and R. Spagna, J. Appl. Crystallogr. **38**, 381 (2005).
[40] Effect of electron transfer interaction may affect the result based on the simple localized-orbital picture, in particular, in the two-dimensional case where the energy gain due to the anisotropic hopping becomes strongly orbital dependent. Therefore, the obtained results might include some error at a quantitative level in a strict sense. However, in view of the excellent agreement of the obtained results with the result of Refs. 18 and 27, the error would not be significant.
[41] J. Kanamori, J. Appl. Phys. **31**, S14 (1960).
[42] The average bond length $\bar{d}$ for $Mn^{3.5+}$ is estimated from the fitting of valence-distance (Mn-O bond length) curves calculated by the bond valence sum of Mn^{3+} and Mn^{4+}.
[43] I. D. Brown and D. Altermatt, Acta Crystallogr. B **41**, 244 (1985).
[44] The calculated bond valence sum for oxygen shows a value of -2 ± 0.1 for all materials, indicating that doped number is well included in the calculated nominal valence of Mn ions. However, it should be noted that doped holes have strong O $2p$ character in reality.
[45] J. Rodríguez-Carvajal, G. Rousse, C. Masquelier, and M. Hervieu, Phys. Rev. Lett. **81**, 4660 (1998).
[46] J.-S. Zhou and J. B. Goodenough, Phys. Rev. Lett. **96**, 247202 (2006).
[47] E. J. Cussen, M. J. Rosseinsky, P. D. Battle, J. C. Burley, L. E. Spring, J. F. Vente, S. J. Blundell, A. I. Coldea, and J. Singleton, J. Am. Chem. Soc. **123**, 1111 (2001).
[48] Minimal disorder effect is also manifested by the absence of enhancement of the atomic displacement factors [see tables in the Appendix and EPAPS (Ref. 49)], ensuring the validity of using bond valence sum analysis.
[49] See EPAPS Document No. E-PRBMDO-80-012930 for Crystallographic Information File (CIF) data with crystal structural data. For more information on EPAPS, see http://www.aip.org/pubservs/epaps.html.
[50] Averaged value of V is 3.61 for $Pr_{0.5}Ca_{0.5}MnO_3$, and is larger than the nominal value of 3.5. Similar tendency is also found for the single-layer and the double-layer compounds. This would be due to the compressed (stretched) nature of Mn-O (rare-earth/alkaline-earth-O) bond and the resultant charge transfer from Mn site to the rare-earth/alkaline-earth site.
[51] J. D. Jorgensen, B. Dabrowski, S. Pei, D. R. Richards, and D. G. Hinks, Phys. Rev. B **40**, 2187 (1989).